Physica E: Low-dimensional Systems and Nanostructures 114 (2019) 113648

Contents lists available at ScienceDirect

Physica E: Low-dimensional Systems and Nanostructures

journal homepage: www.elsevier.com/locate/physe

Ab-initio calculations of strain induced relaxed shape armchair graphene nanoribbon

Sanjay Prabhakar[a,*], Roderick Melnik[a,b]

[a] The MS2Discovery Interdisciplinary Research Institute, M2NeT Laboratory, Wilfrid Laurier University, Waterloo, ON N2L 3C5, Canada
[b] BCAM, Alameda Mazarredo 14, 48080, Bilbao, Spain

A B S T R A C T

An odd number of zigzag edges in armchair graphene nanoribbons and their mechanical properties (e.g., Young's modulus, Poisson ratio and shear modulus) have potential interest for bandgap engineering in graphene based optoelectronic devices. In this paper, we consider armchair graphene nanoribbons passivated with hydrogen at the armchair edges and then apply the strain for tuning the bandgaps. Using density functional theory calculations, our study finds that the precise control of strain can allow tuning the bandgap from semiconductor to mettalic and then again switching back to semiconductor. In addition, we also show that the strained graphene nanoribbon passivated with hydrogen molecules can have large out-of-plane deformations demonstrating the properties of relaxed shape graphene. We express the strain induced by hydrogen in terms of binding energy. Finally, we characterise the effect of strain on the mechanical properties that can be used for making straintronic devices based on graphene nanoribbons.

1. Introduction

The thinnest two dimensional (2D) materials, e.g., graphene, $MoSe_2$ and other TMDs materials have potential interest for making next generation optoelectric, spintronic, straintronic devices that might have performance better than conventional silicon devices [1–8]. For example, the measurement of charge mobility in the graphene CMOS devices is far better than the best silicon devices [7,9–13]. Evidence from experimental measurements confirmed that 2D materials possess unique physical properties, e.g. half integer quantum Hall effect, non-zero Berry curvature and Zak's phase, high mobility charge carriers [7,9,14–17]. Although graphene as a material is exciting at the level of making optoelectronic devices, its bandgap opening is still one of the biggest challenges, e.g. graphene does not have any bandgaps at the Dirac point. However, by using several state-of-the-art techniques and possibility of considering different 2D materials, e.g. $MoSe_2$, one can easily control the bandgaps. Also, a small bandgap opening in graphene is achieved by considering the effect of spin-orbit coupling, strain and magnetic field. One can also make optoelectronic devices from armchair graphene nanoribbons, which possess a large bandgap opening at the Γ-point [18–23]. In these armchair graphene nanoribbon devices, bandgaps can be created in a desired fashion by precise control of the width of the nanoribbon.

Strain engineering in graphene is promising for straintronic and spintronic applications. Possible ways of creating strain in graphene is to modify the in-plane and out-of-plane deformations among the carbon atoms. For examples, in plane and out-of-plane deformations in graphene can lead to the formation of relaxed shape graphene [24–26]. When graphene is relaxed due to precise edge engineering, the localized eigenstates, created due to strain engineering, can lead to several observed interesting phenomena such as conduction and valence band crossings, spin hot spots as well as measurements of decoherence time [24,25,27,28]. Large in-plane and out-of-plane deformations can also be made by growing graphene on a flexible substrate, where not only the lattice mismatch between graphene and the substrate induces strain but also the flexible substrate can be bended for the purpose of inducing strain [29,30]. Ripples and wrinkles in graphene are also of potential interest for band engineering applications [24,25,31–34]. Edge functionalization of graphene nanoribbons by -H, -H_2, -O, -Br can also lead to in-plane and out-of-plane deformations and can be used for engineering of graphene bandgaps [31,35–38].

The mechanical properties, e.g. the Poisson ratio, Young's and shear modulii, of graphene have been characterized by using both experimental and theoretical techniques [26,39–49]. The experimental value of Young's modulus of bulk graphite is 0.02 TPa [50] but its value for stack of graphene sheets is 0.5 TPa [51], for a monolayer of graphene oxide is 0.15 TPa [52] and for a free-standing monolayer graphene membrane is 0.1 TPa [53]. In Ref. [53], authors also reported that the intrinsic breaking strength of graphene as 10 GPa. Ab initio calculations of graphene find the value of Young's modulus to be 1.11 TPa in Ref. [54] and to be 1.24 TPa in Ref. [55], where thickness of graphene is 0.34 nm. By using the semiempirical nonorthogonal tight-binding (TB)

* Corresponding author.
E-mail address: sprabhakar@wlu.ca (S. Prabhakar).

https://doi.org/10.1016/j.physe.2019.113648
Received 18 May 2019; Received in revised form 11 July 2019; Accepted 19 July 2019
Available online 19 July 2019
1386-9477/

method, the Young's modulus of graphene is reported as 1.206 TPa [56]. In summary, the values of Young's modulus reported recently are in close agreement between experimental and theoretical studies within numerical errors [57–61]. Hence, it is confirmed that the values of Young's modulus are extremely large in comparison to other conventional semiconductor materials. Therefore, finding the value of graphene Young's modulus in several different conditions is important for the applications in designing the devices for straintronic, spintronic and optoelectronic applications.

In this paper, we consider armchair graphene nanoribbons functioning their armchair edges by -H and -H_2. We then apply compressive strain to the system along y-direction and tensile strain along x-direction. This leads with possible application connected with opening and closing the bandgaps. In other words, the armchair graphene nanoribbons can be used for dual purposes of semiconductor and metallic. Within density functional theory calculations, our study show that the graphene and graphene with -H functional group can not induce significant values of out-of-plane deformations while graphene with -H_2 functional group does induce large out-of-plane deformations exhibiting the properties of relaxed shape graphene [26]. Such strain engineering can lead to tuning the bandgaps from semiconductor to metal and then again switching back to semiconductor. The binding energy calculations of hydrogen on graphene allow to quantify the effect of strain on the bandengineering of graphene nanoribbons. Finally, we discuss the effect of strain on the Poisson ratio, Young's and shear modulii of graphene nanoribbons.

The paper is organized as follows. In Sec. 2, we provide computational details of density functional theory calculations for generating strain on graphene nanoribbon. In Sec. 3, we present the results for bandengineering, poisson ratio, Young's and shear modulii of graphene, graphene edge functioning with H and H_2. Finally, in Sec. 4, we summarize our results.

2. Computational methods

Density Functional Theory (DFT) calculations for 7 zigzag edges of armchair graphene nanoribbons are performed in the Quantum Espresso software package [62], where periodic boundary conditions are implemented in the simulations. Ultrasoft pseudopotentials and plane wave basis set with a kinetic energy and charge density cut-off at 100Ry and 800Ry are used. We include exchange and correlation effects within the Perdew-Burke-Ernzerhof (PBE) Functional [63]. van der Waals interactions are also included with the Semiempirical Grimme's DFT-D2 corrections term [64]. We use orthorhombic 4.34 Å × 24.78 Å × 15.01 Å size of supercell that contains 7 zigzag edges of an armchair graphene nanoribbon. In the supercell, we have 14 atoms for the graphene nanoribbon, 18 atoms for the graphene nanoribbon with armchair edge functioning with H and 22 atoms for the graphene nanoribbon with armchair edge functioning with H_2. During geometry optimization, all atoms in all the three directions and x-axis of the supercell are fully relaxed until the forces on atoms are smaller than 0.01 eV/Å. We have tested several k-point samplings and calculations are performed at (6,1,3) *k*-points sampling fulfilling the above convergence criteria. The optimized lattice parameters along the x-direction are 4.34 Å for graphene, 4.29 Å for graphene with armchair edge functioning with H, 4.30 Å for graphene with armchair edge functioning with H_2. The optimized widths (distance between C-C atoms) of 7 zigzag edges of armchair graphene nanoribbons are 7.1353 $\AA$ (bare graphene), 7.33 Å(graphene edge functioning with H), 7.56 $\AA$ (graphene edge functioning with H_2). The XCRYSDEN program was used to draw the molecular structure [65]. For strain engineering of graphene nanoribbons, we have applied the compressive stress through the armchair edge and then frozen the y-coordinates of the armchair edge atoms while allowing the other coordinates to be fully relaxed. We also fully relaxed the x-axis of the supercell.

3. Results and discussions

Bandgaps of the armchair graphene nanoribbon depend on the width of the ribbon. If the armchair nanoribbon contains an odd number of zigzag edges then the armchair graphene nanoribbon possesses a finite bandgap opening at the Γ point and interesting for making semiconductor devices. For an even number of zigzag edges, the armchair graphene nanoribbon has a zero band gap opening and thus possesses metallic properties. When strain is implemented in the armchair graphene nanoribbon with odd number of zigzag edges, then width of the graphene nanoribbon either decreases or increases depending on which kind of strain is applied at the boundaries of the nanoribbon. Hence, large modification of band gaps are expected due to application of strain. For example, strain induced by compressive stress reduces the width of the ribbon while tensile stress increases the width of the ribbon. Since the bandgap of graphene nanoribbon depends on the width of the ribbon, we expect the fine tuning of bandgaps with application of strain from semiconductor to metal or viceversa. In this paper, we are interested in tuning the bandgap from a semiconducting to metallic and then bringing it back to the semiconductor with the application of strain engineering. Hence, we consider the 7 zigzag edges of the armchair graphene nanoribbon and then apply the compressive stress at the armchair edge. The armchair ribbon is also allowed to elongate in the x-direction. The schematics of the strained armchair graphene nanoribbon is shown in Fig. 1. One may consider 9, 11, 14 and so on and so forth armchair GNRs and then apply similar kind of compressive stress at the armchair edges for tuning the bandgaps. However in this case, the bandgaps opening at Γ-point is smaller than 7 armchair GNRs and thus we expect bandgap closing at lower values of strain. On the other hand, one may consider 5 and 3 armchair GNRs but the bandgap opening in such nanoribbon is larger than 7 armchair GNRs and hence one may need to apply large strain (larger than 18% as seen zero band gap in 7 armchair GNRs) to close the bandgaps, which may be impractical for the experiment. It is also possible to consider the odd number of armchair edges of the GNRs and then apply the strain so that one can tune the properties of bandgaps from metal to semiconductor.

In Fig. 2, we have plotted the isosurface charge distributions on 7 zigzag edges of armchair GNRs for three different cases: (i) bare GNRs (Fig. 2 (a)), (ii) GNRs with H at the armchair edge (Fig. 2 (b)) and (iii) GNRs with H2 at the armchair edge. As can be seen in Fig. 2, the distributions of isosurface charge in these GNRs are different because different functional groups in GNRs induce slightly different strains. Hence bandgap opening of these ribbons are expected to be different. The bandstructures and density of states of these GNRs are shown in Fig. 3. Irregularities in the mesh grid throughout the structure of GNRs may cause to induce some sharp peaks in the density of states plots in Figs. 3 and 5. At Γ point, we find that the bandgaps of GNRs are 1.36eV for bare GNRs, 1.57eV for GNRs with H and 0.42eV for GNRs with H_2. Since all the GNRs has 7 zigzag edges but different bandgap openings, it clearly indicates that the attachment of hydrogen at the armchair edge plays an important role in the bandgap engineering. More precisely,

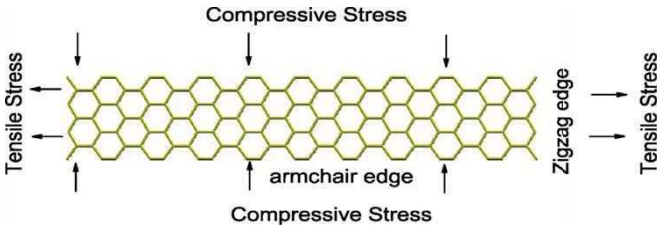

Fig. 1. Schematics of 7 zigzag edges of armchair graphene nanoribbon. We apply compressive stress at the armchair edge while tensile stress at the zigzag edge. Such type of strain engineering allow us to investigate the influence of strain on the bandengineering of graphene nanoribbon.

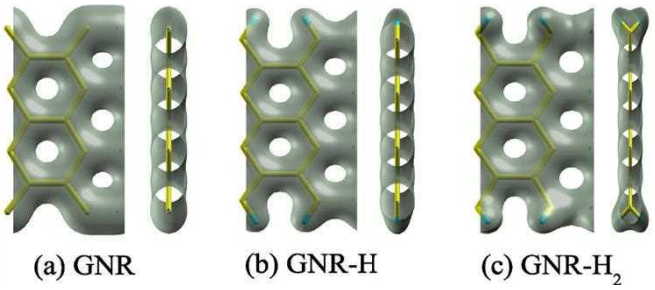

Fig. 2. Isosurface charge distributions of armchair graphene nanoribbon for (a) bare graphene (b) armchair edge functioning with hydrogen (H) and (c) armchair edge functioning with hydrogen molecule ($-H_2$). The isovalue of isosurface charge density is chosen as 0.5.

decorating the armchair edge with different elements modify the band gaps significantly due to modification of the width of the ribbon as well as inducing both in-plane and out-of-plane ripples. For example, the attachment of hydrogen changes the width, (d(C-C)), of the ribbon (7.13 Å vs 7.32 Å vs 7.54 Å) and also induces the in-plane and out-of-plane deformations [36].

The tuning of the bandgaps from semiconductor to metal and bring it back to semiconductor can be achieved by applying external strain through the armchair edge, as shown schematically in Fig. 1. The bandgap engineering with respect to strain is shown in Fig. 4. In Fig. 4 (diamond), we find that graphene always stays as a semiconductor even for large values of strain. On the other hand, in Fig. 4(circle) the armchair edge passivated with hydrogen become metallic (i.e., no bandgap) approximately at 18% of applied strain. The bandgap closing can be achieved even at much smaller values of strain (approximately at 3% of strain) for the case of graphene nanoribbon passivated with H_2. The bandgap closing can be seen due to the effect of strain because applied strain decreases the width of the ribbon. When the ribbon width becomes closer to the width of the 6 (even number) zigzag edge armchair graphene nanoribbon then the metallic behavior in the band engineering of graphene nanoribbon can be seen [66,67].

Using finite element method simulations, authors in Refs. [25,26] have shown that the relaxed shape graphene nanoribbon has potential interest for graphene-based strain engineering devices [26] as well as for the observation of quantum phenomena e.g. discrete energy levels, pseudospin decoherence time and nontrivial topological phases [16,24,66,67]. When the out-of-plane deformations are large as can be

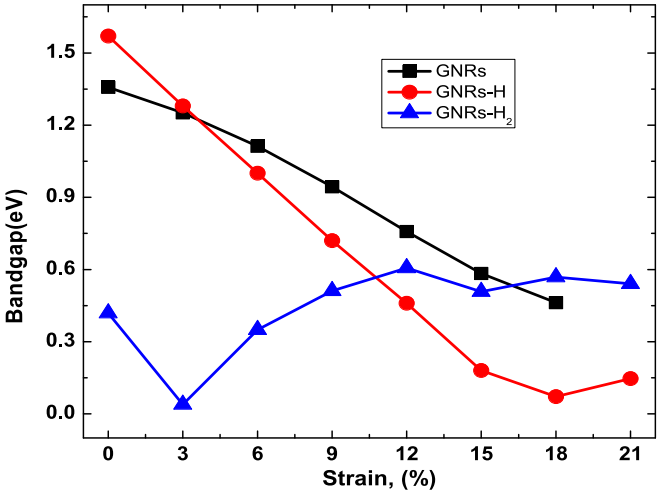

Fig. 4. Band engineering in the armchair graphene nanoribbon with the application of strain in three cases: (a) graphene nanoribbon, (b) graphene nanoribbon functioning with hydrogen at the armchair edge and (c) graphene nanoribbon functioning with H_2 molecule at the armchair edge. We see that the bandgap completely closes at the particular value of strain for the case of graphene nanoribbons functioning with H and H_2. Here, the magnitude of strain is measured as a reference from unstrained GNRs (Fig. 3) by applying compression stress through the armchair edges (Fig. 1).

seen in Fig. 5(a) for the case of graphene passivated with hydrogen, we observe a relaxed shape graphene nanoribbon. In Fig. 5(b) we have plotted the density of states and find the bandgap reopening in the graphene nanoribbon.

Now we turn to the discussions of mechanical properties observed in the armchair graphene nanoribbon due to externally applied compressive strain from the y-direction and tensile strain in the x-direction.

In Fig. 6(a), we plot the relative total energy density (i.e., energy density difference relative to graphene). This total energy is used to calculate the Young's modulus, shear modulus and the binding energy of hydrogen. In this figure, we find that the total energy density increases significantly for the case of graphene passivated with $-H_2$ molecules (circles) at 12% of strain which provides an indication of relaxed shape graphene (i.e., very large out-of-plane deformations) [26]. In Fig. 6 (b), we plot the binding energy of hydrogen in the graphene. The binding energy calculation allows us to characterise

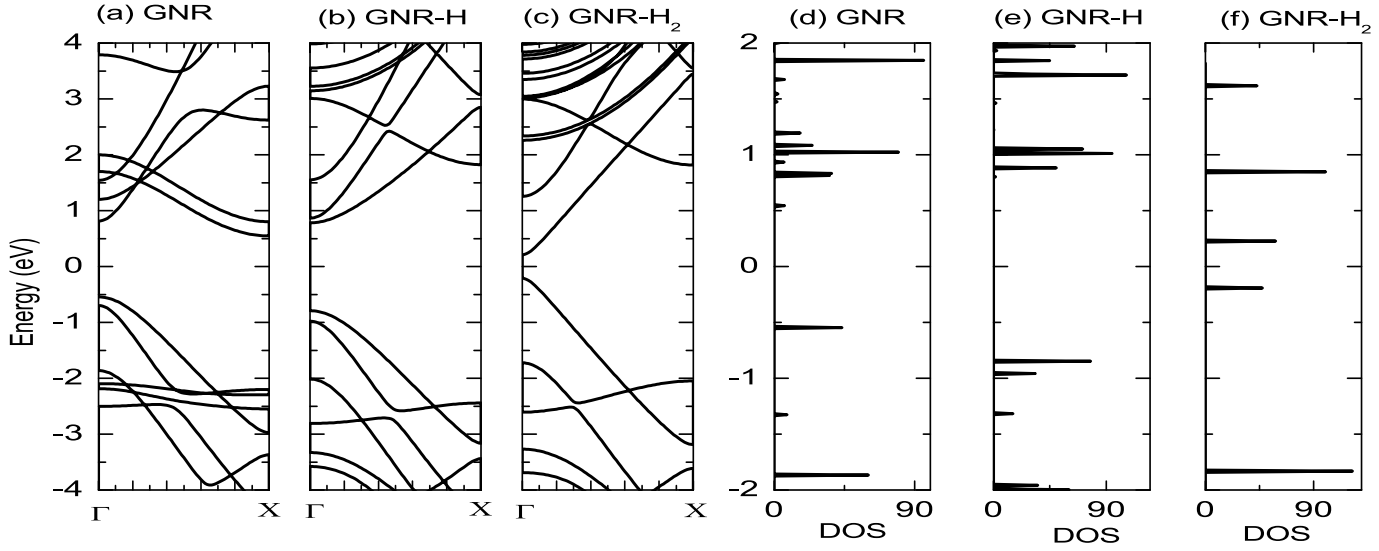

Fig. 3. Band structures and Density of States (DOS) of graphene nanoribbon, graphene nanoribbon armchair edge functioning with H, and graphene nanoribbon armchair edge functioning with H_2.

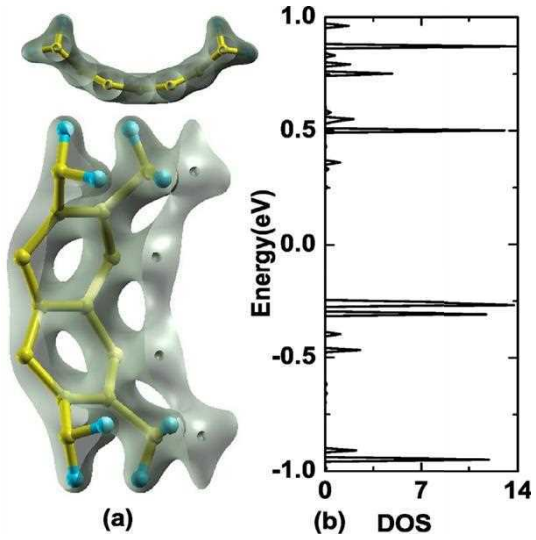

Fig. 5. Isosurface charge distribution in (a) and energy vs density of states in (b) of armchair graphene nanoribbon for armchair edge functioning with hydrogen molecule ($-H_2$) under 15% compressive strain. Notice that the out-of-plane deformations are significantly large that provided the relaxed shape graphene nanoribbon similar to Refs. [25,26]. The isovalue of isosurface charge density is chosen as same as to be in Fig. 2.

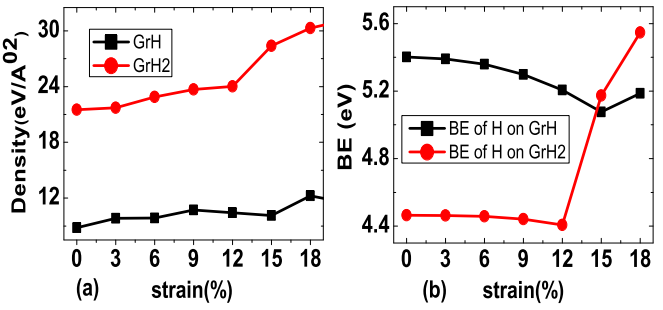

Fig. 6. The variation of relative total energy density vs strain in (a) and binding energy of hydrogen on armchair edge of graphene vs strain in (b). The relative total energy is obtained by subtracting the total energy of the graphene nanoribbon from the total energy of graphene nanoribbon with $-H$ (diamond-black in Fig. 6(a)) and $-H_2$ (circle-red in Fig. 6(a)). (For interpretation of the references to color in this figure legend, the reader is referred to the Web version of this article.)

whether H or H2 is energetically favourable to the armchair edge of the graphene nanoribbon. The binding energy is found by using the expression: [68]

$$BE = U[Gr(H, H_2)] - U[Gr] - U[H], \tag{1}$$

where BE is the binding energy, $U[Gr(H, H_2)]$ is the total energy of graphene with passivation layer, $U[Gr]$ is the total energy of graphene and $U[H]$ is the total energy of hydrogen in vacuum. As can be seen in Fig. 6 (b), the binding energy of hydrogen in the graphene passivated with $-H_2$ enhances significantly after 12% of strain, which provides a clear indication of very large out-of-plane deformations, as can be seen in the optimized structure in Fig. 5. As can be seen in Fig. 6(b), the binding energy of H on graphene-H is larger than H on graphene-H_2 (approximately less than 12% strain) and hence hydrogen on graphene-H is energetically more favourable. However, when the out-of-plane deformations are large due to large strain then the binding energy of H on graphene-H2 is larger and hence H_2 functional group become energetically more favourable.

Finally, we investigate the effect of strain on the Young's modulus, Poisson ratio and shear modulus of graphene nanoribbon. The Young's

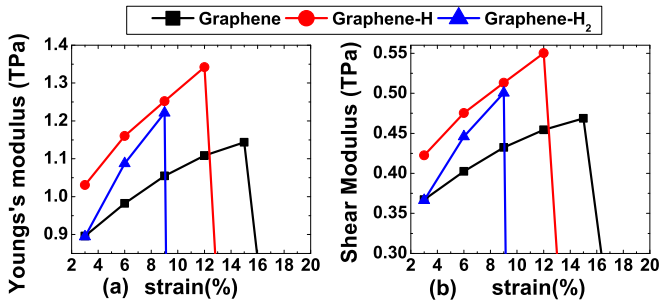

Fig. 7. The variation of Young's modulus with respect to strain in (a) and shear modulus vs strain in (b). Evidently, Young's and shear modulii increase as we increase the strain until they reach their saturation values. The Young's modulus is calculated by using Eq. (2) and shear modulus is calculated by the use of Eq. (3). Here we consider the Poisson ratio, $\nu = 0.22$.

modulus is calculated by using the expression [41]

$$Y = \frac{1}{A_0}\frac{d^2U}{d\epsilon_y^2}, \tag{2}$$

where A_0 is the optimized area without imposing any strain, U is the total energy, and ϵ_y is the externally applied compressive strain. In Fig. 7(a), we find that the Young's modulus of graphene passivated with H_2 is larger than the Young's modulus of graphene and graphene passivated with H. Young's modulus also increases as we increase the strain and then sharply decreases providing an indication of saturation value of the Young's modulus. The numerical values of Young's modulus presented in Fig. 7(a) are consistent with the experimental and theoretical values reported in the literature [26,41–48].

The Poisson ratio is another important physical quantity characterizing the mechanical properties of materials [41–43,69]. By applying compressive external strain, ϵ_y, in the graphene in the y-direction, and by using the supercell of DFT calculations to record the resulted strain in the x-direction, ϵ_x, we find the Poisson ratio from the expression, $\nu = \epsilon_x/\epsilon_y$ as $\nu = 0.25$ for graphene, $\nu = 0.25$ for graphene passivated with H and $\nu = 0.22$ for graphene passivated with H_2. Since the Poisson ratios for all three cases are almost the same ($\nu = 0.25$ (Gr), 0.25 (Gr-H), and 0.22 (Gr-H_2)), we can draw a conclusion that the Poisson ratio of graphene is unaffected by the passivation of -H and H_2 at the armchair edge.

After calculating the Young's modulus and Poisson ratio, we can finally find the shear modulus, G, by using the expression,

$$G = \frac{Y}{2(1+\nu)}. \tag{3}$$

The shear modulus with respect to applied compressive strain is plotted in Fig. 7(b). Similar to Young's modulus, shear modulus also increases as we increase the strain until it reaches to the saturation value.

4. Conclusion

In summary, we have studied the effect of strain on the band engineering (e.g., semiconductor vs mettalic) and the mechanical properties (e.g. Young's modulus, shear modulus and Poisson ratio) of armchair graphene nanoribbons passivated with hydrogen and hydrogen molecules at the armchair edges. We have shown that the strain can be used for tuning the bandgap from semiconductor to metallic, and then strain can again be used to tune the bandgaps from metallic characteristics to semiconductor. We have also shown that at the large values of strain in graphene nanoribbons passivated with hydrogen molecules, large out-of-plane deformations in graphene nanoribbon can show the properties of relaxed shape graphene. We have quantified the strain induced by hydrogen molecules on graphene nanoribbons in terms of the binding energy. Finally, we have shown that the Young's

and shear modulii increase as we increase the strain until they reach to their maximum values while the Poisson ratio is independent to the passivation materials. Our findings of bandgap tuning and exploration of mechanical properties can be used in designing novel optoelectronic devices, as well as for straintronic applications.

Conflicts of interest

There is no conflict of interest.

Acknowledgments

The authors acknowledge the support made by Canada Research Chair Program and National Research Council Canada. The computations were performed utilizing the facilities available on the SHARCNET Supercomputer (www.shracnet.ca) and Compute Canada supercomputer (www.computecanada.ca).

Appendix A. Supplementary data

Supplementary data to this article can be found online at https://doi.org/10.1016/j.physe.2019.113648.

References

[1] C. Androulidakis, E. Koukaras, M. Poss, K. Papagelis, C. Galiotis, S. Tawfick, Phys. Rev. B 97 (2018) 241414.
[2] A. Mannix, Z. Zhang, N. Guisinger, B. Yakobson, M. Hersam, Nat. Nanotechnol. 13 (2018) 444.
[3] R. Wu, I.K. Drozdov, S. Eltinge, P. Zahl, S. Ismail-Beigi, I. Božović, A. Gozar, Nat. Nanotechnol. 1 (2018).
[4] L. Feng, K. Yabuoshi, Y. Sugimoto, J. Onoda, M. Fukuda, T. Ozaki, Phys. Rev. B 98 (2018) 195311.
[5] A.K. Geim, K.S. Novoselov, Nat. Mater. 6 (2007) 183.
[6] J.N. Coleman, M. Lotya, A. O'Neill, S.D. Bergin, P.J. King, U. Khan, K. Young, A. Gaucher, S. De, R.J. Smith, I.V. Shvets, S.K. Arora, G. Stanton, H.-Y. Kim, K. Lee, G.T. Kim, G.S. Duesberg, T. Hallam, J.J. Boland, J.J. Wang, J.F. Donegan, J.C. Grunlan, G. Moriarty, A. Shmeliov, R.J. Nicholls, J.M. Perkins, E.M. Grieveson, K. Theuwissen, D.W. McComb, P.D. Nellist, V. Nicolosi, Science 331 (2011) 568.
[7] N. Savage, Nature 483 (2012) S30.
[8] S. Manzeli, D. Ovchinnikov, D. Pasquier, O.V. Yazyev, A. Kis, Nature Rev. Mater. 2 (2017) 17033.
[9] K.S. Novoselov, A.K. Geim, S.V. Morozov, D. Jiang, Y. Zhang, S.V. Dubonos, I.V. Grigorieva, A.A. Firsov, Science 306 (2004) 666.
[10] L. Liao, Y.-C. Lin, M. Bao, R. Cheng, J. Bai, Y. Liu, Y. Qu, K.L. Wang, Y. Huang, X. Duan, Nature 467 (2010) 305.
[11] T. Yang, B. Zheng, Z. Wang, T. Xu, C. Pan, J. Zou, X. Zhang, Z. Qi, H. Liu, Y. Feng, et al., Nat. Commun. 8 (2017) 1906.
[12] J.S. Friedman, A. Girdhar, R.M. Gelfand, G. Memik, H. Mohseni, A. Taflove, B.W. Wessels, J.-P. Leburton, A.V. Sahakian, Nat. Commun. 8 (2017) 15635.
[13] A. Altıntaş, K. Çakmak, A.D. Güçlü, Phys. Rev. B 95 (2017) 045431.
[14] K.S. Novoselov, A.K. Geim, S.V. Morozov, D. Jiang, M.I. Katsnelson, I.V. Grigorieva, S.V. Dubonos, A.A. Firsov, Nature 438 (2005) 197.
[15] K.S. Novoselov, D. Jiang, F. Schedin, T.J. Booth, V.V. Khotkevich, S.V. Morozov, A.K. Geim, PNAS 102 (2005) 10451.
[16] T. Cao, F. Zhao, S.G. Louie, Phys. Rev. Lett. 119 (2017) 076401.
[17] G.D. Nguyen, H.-Z. Tsai, A.A. Omrani, T. Marangoni, M. Wu, D.J. Rizzo, G.F. Rodgers, R.R. Cloke, R.A. Durr, Y. Sakai, et al., Nat. Nanotechnol. 12 (2017) 1077.
[18] M.Y. Han, B. Özyilmaz, Y. Zhang, P. Kim, Phys. Rev. Lett. 98 (2007) 206805.
[19] S.Y. Zhou, G.-H. Gweon, A. Fedorov, d. First, PN, W. De Heer, D.-H. Lee, F. Guinea, A.C. Neto, A. Lanzara, Nat. Mater. 6 (2007) 770.
[20] F. Xia, D.B. Farmer, Y.-m. Lin, P. Avouris, Nano Lett. 10 (2010) 715.
[21] Y.-C. Chen, T. Cao, C. Chen, Z. Pedramrazi, D. Haberer, D.G. De Oteyza, F.R. Fischer, S.G. Louie, M.F. Crommie, Nat. Nanotechnol. 10 (2015) 156.
[22] M.M. Ugeda, A.J. Bradley, S.-F. Shi, H. Felipe, Y. Zhang, D.Y. Qiu, W. Ruan, S.-K. Mo, Z. Hussain, Z.-X. Shen, et al., Nat. Mater. 13 (2014) 1091.
[23] L. Brey, H.A. Fertig, Phys. Rev. B 73 (2006) 235411.
[24] S. Prabhakar, R. Melnik, L. Bonilla, Phys. Rev. B 93 (2016) 115417.
[25] S. Prabhakar, R. Melnik, L.L. Bonilla, S. Badu, Phys. Rev. B 90 (2014) 205418.
[26] V.B. Shenoy, C.D. Reddy, A. Ramasubramaniam, Y.W. Zhang, Phys. Rev. Lett. 101 (2008) 245501.
[27] S. Prabhakar, R. Melnik, L. Bonilla, Eur. Phys. J. B 90 (2017) 92.
[28] S. Prabhakar, R. Melnik, J. Phys. Condens. Matter 27 (2015) 435801.
[29] Z.H. Ni, W. Chen, X.F. Fan, J.L. Kuo, T. Yu, A.T.S. Wee, Z.X. Shen, Phys. Rev. B 77 (2008) 115416.
[30] R. Carrillo-Bastos, C. León, D. Faria, A. Latgé, E.Y. Andrei, N. Sandler, Phys. Rev. B 94 (2016) 125422.
[31] H. Lim, J. Jung, R.S. Ruoff, Y. Kim, Nat. Commun. 6 (2015) 8601.
[32] M.S. Bronsgeest, N. Bendiab, S. Mathur, A. Kimouche, H.T. Johnson, J. Coraux, P. Pochet, Nano Lett. 15 (2015) 5098.
[33] E. Cerda, L. Mahadevan, Phys. Rev. Lett. 90 (2003) 074302.
[34] R.J.T. Nicholl, N.V. Lavrik, I. Vlassiouk, B.R. Srijanto, K.I. Bolotin, Phys. Rev. Lett. 118 (2017) 266101.
[35] T. J. D. Kumar Deepika, A. Shukla, R. Kumar, Phys. Rev. B 91 (2015) 115428.
[36] P. Wagner, C.P. Ewels, J.-J. Adjizian, L. Magaud, P. Pochet, S. Roche, A. Lopez-Bezanilla, V.V. Ivanovskaya, A. Yaya, M. Rayson, et al., J. Phys. Chem. C 117 (2013) 26790.
[37] B. Zeng, Y. Dong, Y. Yi, D. Li, S. Zhang, M. Long, J. Phys. Condens. Matter 31 (2019) 165502.
[38] B. Zeng, M. Long, Y. Dong, J. Xiao, S. Zhang, Y. Yi, Y. Gao, J. Phys. Condens. Matter 31 (2019) 295702.
[39] C.P. Herrero, R. Ramírez, Phys. Rev. B 97 (2018) 195433.
[40] D. Yllanes, S.S. Bhabesh, D.R. Nelson, M.J. Bowick, Nat. Commun. 8 (2017) 1381.
[41] R. Faccio, P.A. Denis, H. Pardo, C. Goyenola, A.W. Mombrú, J. Phys. Condens. Matter 21 (2009) 285304.
[42] J.-W. Jiang, J.-S. Wang, B. Li, Phys. Rev. B 80 (2009) 113405.
[43] H. Zhao, K. Min, N. Aluru, Nano Lett. 9 (2009) 3012.
[44] R.A. Bizao, T. Botari, E. Perim, N.M. Pugno, D.S. Galvao, Carbon 119 (2017) 431.
[45] A. Sgouros, G. Kalosakas, K. Papagelis, C. Galiotis, Sci. Rep. 8 (2018) 9593.
[46] M. Hossain, T. Hao, B. Silverman, J. Phys. Condens. Matter 30 (2018) 055901.
[47] R.J. Nicholl, N.V. Lavrik, I. Vlassiouk, B.R. Srijanto, K.I. Bolotin, Phys. Rev. Lett. 118 (2017) 266101.
[48] M.J. Bowick, A. Košmrlj, D.R. Nelson, R. Sknepnek, Phys. Rev. B 95 (2017) 104109.
[49] D. Wan, D.R. Nelson, M.J. Bowick, Phys. Rev. B 96 (2017) 014106.
[50] O. Blakslee, D. Proctor, E. Seldin, G. Spence, T. Weng, J. Appl. Phys. 41 (1970) 3373.
[51] I. Frank, D.M. Tanenbaum, A.M. van der Zande, P.L. McEuen, J. Vac. Sci. Technol. B: Microelectron. Nanometer Struct. Process., Meas. Phenom. 25 (2007) 2558.
[52] C. Gómez-Navarro, M. Burghard, K. Kern, Nano Lett. 8 (2008) 2045.
[53] C. Lee, X. Wei, J.W. Kysar, J. Hone, Science 321 (2008) 385.
[54] G. Van Lier, C. Van Alsenoy, V. Van Doren, P. Geerlings, Chem. Phys. Lett. 326 (2000) 181.
[55] E. Konstantinova, S.O. Dantas, P.M. Barone, Phys. Rev. B 74 (2006) 035417.
[56] E. Hernandez, C. Goze, P. Bernier, A. Rubio, Phys. Rev. Lett. 80 (1998) 4502.
[57] D.G. Papageorgiou, I.A. Kinloch, R.J. Young, Prog. Mater. Sci. 90 (2017) 75.
[58] A. Falin, Q. Cai, E.J. Santos, D. Scullion, D. Qian, R. Zhang, Z. Yang, S. Huang, K. Watanabe, T. Taniguchi, et al., Nat. Commun. 8 (2017) 15815.
[59] D. Zhu, Y. Ren, G. Liao, S. Jiang, F. Liu, J. Guo, G. Xu, J. Appl. Polym. Sci. 134 (2017) 45332.
[60] G. Wang, Z. Dai, Y. Wang, P. Tan, L. Liu, Z. Xu, Y. Wei, R. Huang, Z. Zhang, Phys. Rev. Lett. 119 (2017) 036101.
[61] K. Choudhary, G. Cheon, E. Reed, F. Tavazza, Phys. Rev. B 98 (2018) 014107.
[62] P. Giannozzi, S. Baroni, N. Bonini, M. Calandra, R. Car, C. Cavazzoni, D. Ceresoli, G.L. Chiarotti, M. Cococcioni, I. Dabo, A. Dal Corso, S. de Gironcoli, S. Fabris, G. Fratesi, R. Gebauer, U. Gerstmann, C. Gougoussis, A. Kokalj, M. Lazzeri, L. Martin-Samos, N. Marzari, F. Mauri, R. Mazzarello, S. Paolini, A. Pasquarello, L. Paulatto, C. Sbraccia, S. Scandolo, G. Sclauzero, A.P. Seitsonen, A. Smogunov, P. Umari, R.M. Wentzcovitch, J. Phys. Condens. Matter 21 (2009) 395502.
[63] J.P. Perdew, K. Burke, M. Ernzerhof, Phys. Rev. Lett. 77 (1996) 3865.
[64] S. Grimme, J. Comput. Chem. 27 (2006) 1787.
[65] A. Kokalj, Comput. Mater. Sci. 28 (2003) 155.
[66] D.J. Rizzo, G. Veber, T. Cao, C. Bronner, T. Chen, F. Zhao, H. Rodriguez, S.G. Louie, M.F. Crommie, F.R. Fischer, Nature 560 (2018) 204.
[67] O. Gröning, S. Wang, X. Yao, C.A. Pignedoli, G. Borin Barin, C. Daniels, A. Cupo, V. Meunier, X. Feng, A. Narita, K. Müllen, P. Ruffieux, R. Fasel, Nature 560 (2018) 209.
[68] S. Prabhakar, R. Melnik, Sci. Rep. 7 (2017) 17365.
[69] I. Burmistrov, I. Gornyi, V.Y. Kachorovskii, M. Katsnelson, J. Los, A. Mirlin, Phys. Rev. B 97 (2018) 125402.